Applied Nanoscience (2020) 10:1555–1569
https://doi.org/10.1007/s13204-019-01230-y

ORIGINAL ARTICLE

Visible light-assisted photodegradation by silver tungstate-modified magnetite nanocomposite material for enhanced mineralization of organic water contaminants

Sanjay Kumar[1] · Alka[1] · Tarun[1] · Jatin Saxena[1] · Chirag Bansal[1] · Pratibha Kumari[1]

Received: 21 October 2019 / Accepted: 2 December 2019 / Published online: 14 December 2019

Abstract
The modification of silica-coated magnetite nanoparticles with silver tungstate has been reported to form an effective heterogeneous photo-Fenton catalyst (Fe@AgW) for wastewater treatment. The prepared nanocomposite was analyzed and characterized with the help of SEM, TEM, Powder XRD, BET, UV-DRS, and FT-IR spectroscopy. The nanocatalyst was successfully investigated for mineralization of model cationic and anionic dyes representing industrial effluents pollution and colorless pollutant bisphenol A. The degradation of methylene blue (MB) and methyl orange (MO) was up to 92% and 82%, respectively, using Fe@AgW nanocomposite as a photo-Fenton catalyst. The nanocatalyst was also tested against pathogenic bacterial strains to explore its broad-spectrum use for water treatment. The material owns its desired properties such as economic, high efficiency, simple reaction conditions, and effortless magnetic separation for its potential broad scope applicability in water treatment.

Keywords Magnetite · Silver tungstate · Visible light photo-fenton catalysis · Wastewater treatment

Introduction

The major world's alarming situations include scarcity of usable water. Industrial effluents, population outgrowth, and agricultural activities are majorly responsible for water contamination (Kummu et al. 2016). Industrial effluents, including dyes and other organic materials, are highly dangerous in terms of ecological imbalance since they lead to restrain photosynthesis by restricting light penetration (Garg et al. 2004) and are potent carcinogens to mammals (Fisher 1999; Olliver et al. 2003). Infectious microorganisms like Gram-negative (Thune et al. 1993) and Gram-positive bacteria (Emmert and Handelsman 1999) cause various health hazards (Li et al. 2000) and, thereby, their destruction from water bodies has also become crucial for water treatment strategies. Cationic and anionic dyes constitute a significant portion of water contaminants due to their widespread use and then their discharge into water bodies. Methylene blue (MB) and methyl orange (MO) dyes belong to the most commonly used cationic and anionic dyes, respectively. MB is well known to affect the central nervous system (Vutskits et al. 2008) and the toxicity of MO has also been reported in aqueous solution (Xie et al. 2016). Bisphenol A (BPA) is another persistent water contaminating chemical which is commonly present in various materials used in everyday life such as electronic equipment, toys, water pipes, paper and, thus, consumers frequently exposed to it through food and drinking water. The increased amount of BPA in the environment leads to its hazardous endocrine-disrupting effects (Michałowicz 2014). Thereby, the development of the mineralization strategy of these contaminants through effective, economical, simple and easy method has become a smouldering issue with saving the environment.

Various water remediation approaches such as nanofiber microfiltration (Gopakumar et al. 2017), oxidation (Särkkä et al. 2015), biological trickling filters (Abou-Elela et al. 2017; Tatoulis et al. 2017), adsorption (Gjipalaj and Alessandri 2017), bio-sorption (Crini et al. 2018), reverse osmosis (Wenhai Luo et al. 2017), photocatalysis (Singh et al. 2013; Srikanth et al. 2017) and membrane filtration (Dickhout et al. 2017) have been developed to address the issue of wastewater. The advanced oxidation processes (AOPs)

✉ Pratibha Kumari
pkumari@db.du.ac.in; pratibhatanwar77@gmail.com

[1] Department of Chemistry, Deshbandhu College, University of Delhi, New Delhi, India

involving Fenton's reagent (Bokare and Choi 2014) are gaining much more research interest in water remediation applications due to its effectiveness and ease (Pirkanniemi and Sillanpää 2002; Soon and Hameed 2011). In recent years, magnetite-based nanomaterials have been widely developed and utilized as an efficient Fenton-like catalyst for the degradation of organic contaminants in the neutral medium by producing hydroxyl radicals in the presence of hydrogen peroxide (Hongping et al. 2015; Kumari et al. 2018; Wang et al. 2013). The enhanced catalytic activity of magnetite nanoparticles has reported in the literature by coating it with SiO_2 (Yang et al. 2015). The efficiency of the magnetite-based Fenton-like catalytic system is also further enhanced by the presence of ultraviolet light through a photo-Fenton reaction (Pastrana-Martínez et al. 2015).

Nanomaterials have been used worldwide to develop chemical mechanical polishing slurry for the smoothing of nanoparticles surface to enhance their performance and applicability. Recently, many reports have been documented on the development of chemical mechanical polishing slurry using environment friendly materials to make the surface of nanoparticles ultra smooth for their better performance. The newly developed chemical mechanical slurry for copper (Zhang et al. 2019), titanium alloy (Zhang et al. 2018), cadmium zinc telluride (Zhang et al. 2016a, b, c) and mercury cadmium telluride (Zhang et al. 2016a, b, c) mainly includes silica, hydrogen peroxide and active biodegradable component such as chitosan, malic acid or citric acid. Many environment friendly approaches have been established which are very crucial for the growth of microelectronics industries and high-performance product manufacturing. The recent advances in nanotechnology have helped to establish original environmentally safe construction protocols and machining tools including diamond wheels and grinders for fabricating high-performance products (Sagapuram et al. 2015; Zhang et al. 2015; Zhang et al. 2012a, b, c; Zhang et al. 2013; Zhang et al. 2012a, b, c). Nanostructures of silicon and silicon carbide devised by nanoscale distortions have also been studied for machine and high-performance devices (Cui et al. 2019a, b; Wang et al. 2018a, b; Zhang et al. 2017). The use of nanomaterials has revolutionized the conventional toxic and harmful machining and manufacturing approaches by environment friendly tools and thereby contamination of environment is drastically reduced. Herein, we developed magnetite-based nanomaterial for its application in environment remediation.

In recent years, magnetite-based nanomaterials have developed as immobilized nanosorbent and as promising redox and photocatalyst long ago because of its low toxicity, cost-effective, coherent activity, and effortless removal (Fan et al. 2012; Kumari et al. 2016, 2018; Kumari et al. 2019; Kumari and Parashara 2018). However, its application in photocatalysis suffers from some limitations such as the inapt bandgap (2.0–2.2 eV) for a visible light application, high electron–hole pair recombination rate, and its high aggregate formation tendency in solution (Boyer et al. 2010). To conquer the issues, the fabrication of magnetite nanoparticles with various photoactive materials such as ZnO and TiO_2 is also reported, which exhibits enhanced photocatalytic activity (Atla et al. 2018; Fakhri et al. 2017; Mishra et al. 2019). However, the Fenton-like activity of magnetite nanocomposites under visible light has not much explored. Recently, numerous magnetic iron-based nanomaterials such as $Ag_2S/BiFeO_3$ (Di et al. 2019), Fe/Si codoped TiO_2 (Du et al. 2018) and Fe-doped ZnS (Wang et al. 2018a, b) have been developed as efficient visible light photo-Fenton catalytic system for environmental remediation applications. There is a growing demand to develop a more efficient, versatile and straightforward photo-Fenton catalyst, driven by visible light.

Silver tungstate (Ag_2WO_4) has been gaining increasing research attention owing to its promising photocatalytic and photoluminescent properties (Xuefei et al. 2013; Zhang et al. 2012a, b, c). Despite these properties, silver compounds have shown susceptibility toward self-consumption since, during the photoirradiation process, chances of metallic silver formation increase (Chen and Xu 2014). Therefore, Ag_2WO_4 has been functionalized with some other surface to make it more photocatalytic adroit (Zhu et al. 2017). Herein, we report the fabrication of SiO_2-coated magnetite nanoparticles with silver tungstate via hydrothermal route and their application in degradation of MB, MO, and BPA as model water contaminants through visible light-assisted photo-Fenton reaction. The antibacterial activity of the prepared nanocomposite has also examined against Gram-positive and Gram-negative bacteria.

Experimental

Materials and methods

The chemicals and reagents used in the preparation of nanomaterials were of commercial (AR) grade and were used without further purification. The transmission electron microscope (TEM) data were recorded using Model FEI Tecnai G2 20 S-twin microscope operating at200 kV. The powder X-ray diffraction (P-XRD) data were recorded on Bruker, D8 Discover, X-ray source Cu. The FT-IR spectra were obtained on Perkin Elmer, Model Spectrum RXI-Mid IR instrument. The scanning electron microscope (SEM) data along with energy-dispersive X-ray spectroscopy (EDX) were obtained using the JEOL-JSM 6610LV instrument. The UV–visible diffuse reflectance spectroscopy (DRS) was performed on Perkin Elmer UV–Vis–NIRLambda 750 spectrophotometer using the polytetrafluoroethylene (PTFE) polymer as a standard. The Brunauer–Emmett–Teller (BET) measurements were carried out on Quantachrome Autosorb-iQ-MP-XR system at 77 K. The photocatalytic procedures were carried out with the help of self-made photoreactor equipped with two 12 W white light-emitting CFL lamps with UV cutoff filters which produce an intensity of approximately 45,000 lx, measured by LX-101A digital lux meter. The UV–visible spectral measurements were carried out on Systronics-117 spectrophotometer in a range from 200 to 800 nm.

Preparation of Fe_3O_4 @SiO_2 nanoparticles

The magnetite nanoparticles (Fe_3O_4) were prepared according to the literature method (Kumari et al. 2016, 2018). In brief, aqueous solution of ammonia (25%, 20 mL) was added to the solution of ferrous chloride (0.43 g) and ferric chloride (1.18 g) in distilled water (20 mL) under nitrogen atmosphere and then the reaction mixture was heated at 70 °C while stirring for 5 h. The black solid of magnetite nanoparticles was separated by centrifugation and washed three times with distilled water followed by ethanol.

The coating of SiO_2 onto the surface of magnetite nanoparticles was carried out by treating nano Fe_3O_4 with tetraethyl orthosilicate (Guo et al. 2015). Magnetite nanoparticles (200 mg) were dispersed in ethanol by ultrasonication for 30 min. The aqueous solution of ammonia (25%, 6 mL) and then 94 mL of distilled water were added sequentially to magnetite suspension. The reaction mixture was sonicated for 40 min and then tetraethyl orthosilicate (1.2 mL) was added at room temperature. The reaction mixture was stirred for 8 h and then the product was separated by centrifugation.

Preparation of Ag_2WO_4 (AgW)

For Ag_2WO_4 synthesis, a solution of 16.98 g of $AgNO_3$ in 500 mL distilled water was mixed dropwise to an aqueous solution of $Na_2WO_4 \cdot 2H_2O$ (16.49 g) in 50 mL distilled water using magnetic stirrer. The resultant solution was stirred magnetically for 24 h at room temperature. The precipitates were separated through vacuum filtration followed by washing with water and then with methanol and dried at 80 °C.

Preparation of Fe_3O_4@SiO_2@Ag_2WO_4 nanocomposite (Fe@AgW)

The Fe_3O_4@SiO_2@Ag_2WO_4 nanocomposite was synthesized through the sonochemical method as follows: 1.586 g of Fe_3O_4@SiO_2 and 0.120 g of Ag_2WO_4 were dispersed in 50 mL of $CHCl_3$ and sonicated for 60 min. Then, the suspension was stirred at room temperature for 12 h. After that, the mixture was filtered and dried at 80 °C for 5 h.

Representative procedure for photo-Fenton degradation reaction of MB/MO/BPA catalyzed by Fe_3O_4@SiO_2@Ag_2WO_4 (Fe@AgW) nanocomposite under visible light

In a typical degradation experiment, 20 mg of nanocomposite (Fe@AgW) was dispersed in 50 mL of aqueous dye solution (3×10^{-5} M) by ultrasonication. The suspension was stirred under dark conditions for 30 min to attain adsorption–desorption equilibrium between dye molecules on the surface of the nanocatalyst. The dye concentration after adsorption–desorption equilibrium was regarded as initial concentration (C_0). Then, 10 mmol H_2O_2 solutions (30%) were added to the suspension and subjected to the visible light irradiation in a homemade photoreactor setup consisting of two 12 W white light-emitting CFL lamps. During photo-Fenton reaction, at regular intervals, small aliquots from the reaction mixture were taken out, and after removing catalyst using a magnet, the concentration of dye was measured at time "t" (C_t) using the UV–Vis spectrophotometer at 464 nm and 664 nm for MO and MB, respectively. The photo-Fenton catalytic degradation rate (%) of dye was calculated by applying the following formula:

$$\text{Degradation rate} = 1 - \frac{C_t}{C_o} \times 100.$$

Antibacterial studies

Agar well diffusion assay

Antibacterial activity of silver tungstate decorated iron oxide nano-composite (Fe@AgW) was evaluated primarily by agar well diffusion assay (Balouiri et al. 2016). Briefly, 90 mm of nutrient agar plates was prepared by pouring sterile nutrient agar into plates and incubated overnight at 37 °C to check their sterility. The next day, log culture of *Staphylococcus aureus, pseudomonas aeruginosa, Klebsiella pneumoniae,* and *Bacillus subtilis* was prepared, and 100 µl of each of culture was plated on nutrient agar plates. The spread cultures were allowed to dry, and wells were prepared by punching nutrient agar in plates. The nanocomposite Fe@AgW (15 mg/ml) was suspended in deionized water and sonicated for 2 min to make homogenous preparation of nanocomposite. 50 µl of nanocomposite solution was loaded into the wells and allowed to diffuse under visible light in the laminar hood for 2 h. Plates were incubated for 18–24 h at 37 °C, and next day plates were observed for the zone of inhibition. The zone of inhibition was measured and recorded as the activity of nanocomposite.

Minimum inhibition concentrations

The minimum inhibition concentration (MIC) was investigated by the micro-broth dilution method as per CLSI guidelines. The nanocomposite (15 mg/ml) was suspended in deionized water and sonicated for 2 min for homogenous preparation. 100 µl of nanocomposite was added to each well with a varying range of concentration (15 mg to 0.11 mg) in a 96-well microtitre plates. Log culture of *S. aureus, P. aeruginosa, K. pneumoniae,* and *B. subtilis* (0.5 OD at 600 nm) was prepared, and 100 µl of each culture was added to the wells. Sterile deionized water was kept as blank along with the tested suspensions. Microtitre plates were incubated at 37 °C for 18–24 h, and next day MIC was determined based on the turbidity of culture in wells. The minimum concentration of nanocomposite which does not show turbidity in tested wells as compared to control well was treated as MIC of the nanocomposite.

Minimum bactericidal concentration

To determine the minimum bactericidal concentration (MBC) of the nanocomposite, the micro-broth dilution method was employed. After MIC, as described in the above section, cultures from each well were plated on nutrient agar media and plates were incubated for 18-24 h at 37 °C. The next day, plates were observed for the viability of cells from each well and MBC was determined. The MBC of nanocomposite is defined as their lowest concentration as compared to control which kills 100% of viable cells.

Since all the pathogenic bacterial strains chosen for accessing the activity of prepared nanocomposite are very harmful and contaminate water resources, all the antibacterial efficacy tests were performed in a sterile laminar hood following the standard conditions. After testing, the bacterial strains were autoclaved and discarded to prevent further environmental hazards.

Results and discussion

Characterization of nanocomposite Fe_3O_4@SiO_2@Ag_2WO_4 (Fe@AgW)

Magnetite nanoparticles were synthesized by chemical co-precipitation method as we have already reported in our recent publication [26] and characterized by different techniques. The powder X-ray diffraction pattern of Fe_3O_4 nanoparticles exhibited diffraction peaks corresponding to (hkl) planes at (220), (311), (400), (511) and (440) (JCPDS# 064829) (Ramírez and Landfester, 2003) which are the characteristics of spinel phase structure of magnetite nanoparticles with a cubic crystal system (Fig. 1). The FT-IR

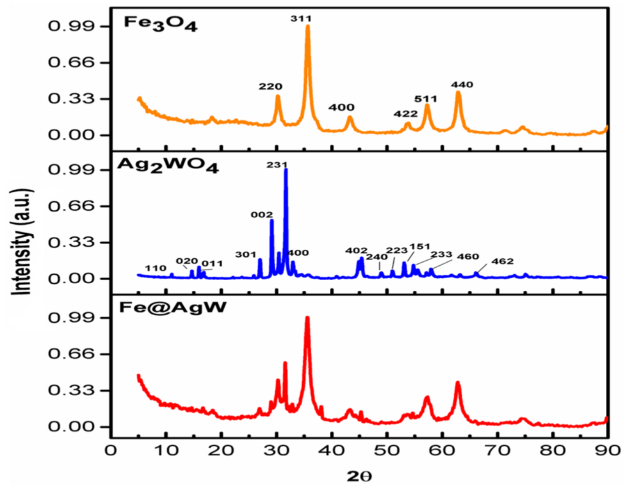

Fig. 1 Powder XRD data of Fe_3O_4, Ag_2WO_4, and Fe@AgW

spectrum of Fe_3O_4 nanoparticles exhibited a strong peak at 3420 cm^{-1} due to –OH bond stretching and at 593 cm^{-1} due to characteristic Fe–O bond stretching, confirming the formation of magnetite nanoparticles (ESI, Fig. 2S). To prevent its agglomeration and to enhance its photocatalytic activity as reported in the literature (Yang et al. 2015), SiO_2 coating onto the surface of magnetite nanoparticles was carried out by the literature method (Guo et al. 2015). The powder X-ray diffraction pattern of Fe_3O_4@SiO_2 exhibited diffraction peaks corresponding to (hkl) planes at (220), (311), (400), (511) and (440) (ESI, Fig. 1S) present in P-XRD of Fe_3O_4, suggesting the presence of magnetite core. The FT-IR spectrum of Fe_3O_4@SiO_2 showed the presence of –Fe–O– stretching band at 596 cm^{-1} along with a band at 1070 cm^{-1} for –Si–O– bond stretching (ESI, Fig. 2S), confirming the presence of SiO_2 coating onto the surface of magnetite nanoparticles. The morphology of Fe_3O_4@SiO_2 was studied by its SEM image (ESI, Fig. 3S) which showed its spherical shape similar to magnetite nanoparticles. The synthesized silver tungstate (AgW) showed rod-like structure in SEM image (ESI, Fig. 4S) and its P-XRD data exhibited all sharp and well-defined diffraction peaks corresponding to the planes (110), (020), (011), (301), (002), (231), (400), (402), (240), (223), (151), (233), (460) and (462) which were observed at 2θ values 10.96, 14.73, 16.74, 28.87, 30.31, 31.59, 32.88, 45.32, 49.05, 51.13, 52.99, 54.66, 57.05 and 65.97 (Fig. 1), respectively, and are coherent with the corresponding planes of Ag_2WO_4 (JCPDS# 34-0061) (Van Den Berg and Juffermans 1982). The Fe_3O_4@SiO_2 nanoparticles were modified with silver tungstate by the sonochemical method and characterized by different data. The P-XRD of Fe@AgW showed the diffraction peaks corresponding to the (hkl) planes of Fe_3O_4 and Ag_2WO_4 (Fig. 1), confirming the grafting of silver tungstate onto Fe_3O_4@SiO_2. The IR spectrum of Fe@AgW showed the characteristic stretching for Fe–O–Fe at 591 cm^{-1} and W–O–W/O–W–O at 634 and 799 cm^{-1} (ESI, Fig. 5S). The investigation of the morphology of the Fe@AgW nanocomposite was carried out by SEM and TEM images analysis (Figs. 2, 3), which clearly showed the affirmativeness of nanoparticles with size ranges from 4 to 7 nm by TEM image. The SEM image of Fe@AgW showed the small-sized nanospheres. The EDX data showed the presence of Ag, W, iron, Si and oxygen which indicated the absence of any impurity in Fe@AgW (Fig. 2b). The HRTEM image shows the presence of lattice fringes having d-spacing 0.28 nm which could be attributed to the (231) plane of Ag_2WO_4 (Fig. 3a). In addition, the lattice fringes having d-spacing of 0.29 nm correspond to the (220) plane of Fe_3O_4, which clearly indicated the grafting of silver tungstate on silica-coated magnetite nanoparticles.

The optical properties of the prepared nanocatalyst were analyzed by measuring UV–Vis diffuse reflectance absorption spectroscopy in the 200–800 nm range (Fig. 4). The UV–Vis diffuse spectra of bare AgW exhibited an absorption edge around 418 nm, which corresponds to its intrinsic bandgap absorption and bandgap energy of 2.96 eV, calculated using the wavelength and energy relation ($\lambda = 1240/E_g$). Bare Fe_3O_4 nanoparticles showed absorption in the whole range of 200–800 nm (Shekofteh-Gohari and Habibi-Yangjeh 2015). Furthermore, the absorption spectra

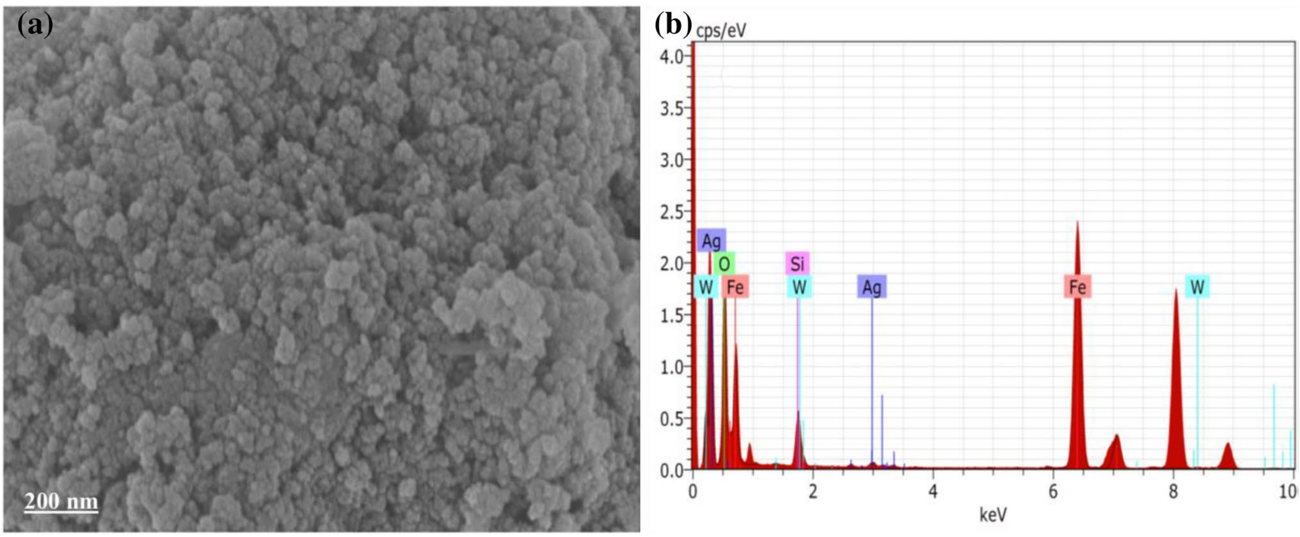

Fig. 2 **a** SEM, **b** EDX of Fe@AgW

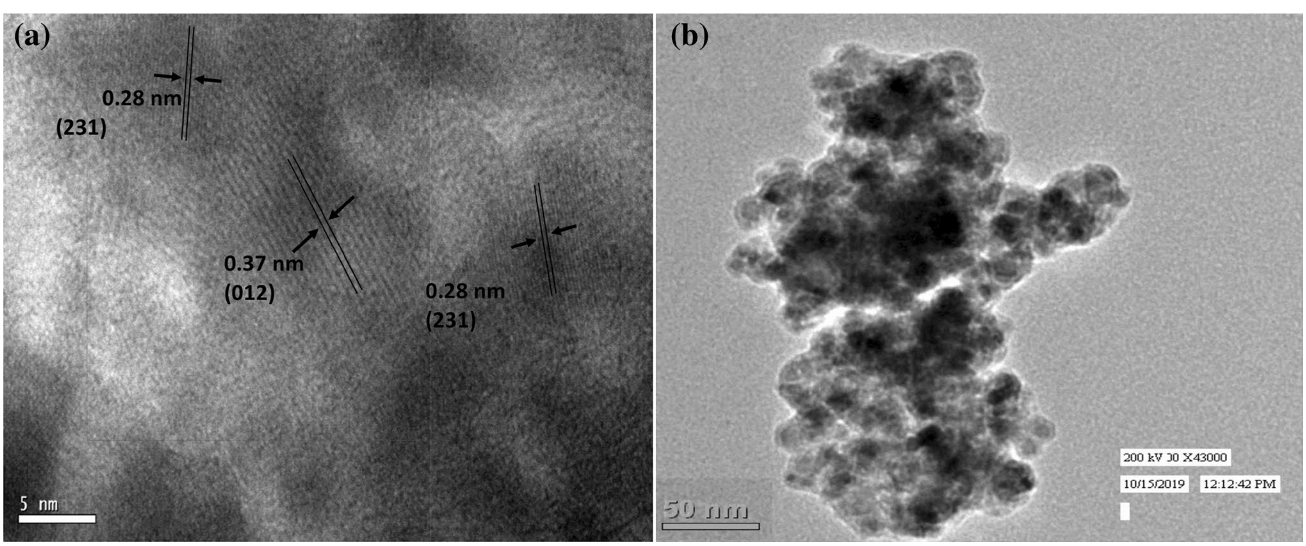

Fig. 3 **a** HR-TEM and **b** TEM of Fe@AgW

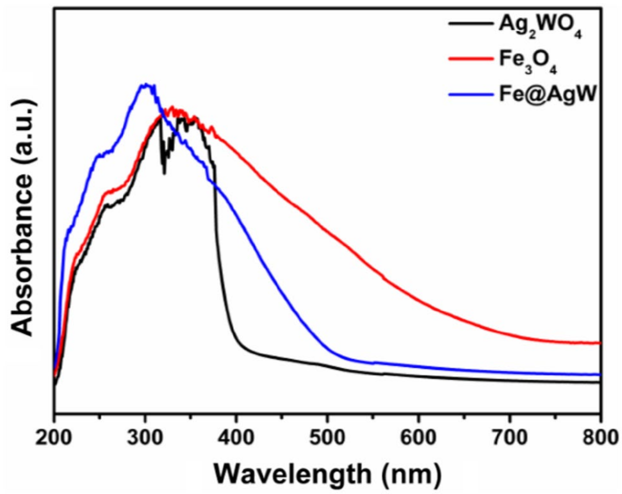

Fig. 4 The UV–Visible diffuse reflectance spectra of Fe_3O_4, Ag_2WO_4, and Fe@AgW

of Fe@AgW nanocomposite exhibited the absorption pattern corresponding to both Fe_3O_4 and Ag_2WO_4. The Fe_3O_4 nanoparticles and Fe@AgW nanocomposite exhibited the bandgap value of 1.75 eV and 2.56 eV, respectively. This bandgap narrowing from 2.96 eV in Ag_2WO_4 to 2.56 eV in Fe@AgW nanocomposites can be attributed to the chemical interactions between Fe_3O_4 and Ag_2WO_4 along with intimate interfacial contact. Figure 5 presents the plot obtained via the transformation based on Kubelka–Munk function vs energy of light (Manikandan et al. 2014) which presents the obtained bandgap values of all prepared catalysts.

As the photocatalytic activity of nanomaterial is related to their available surface area, we performed the Brunauer–Emmett–Teller (BET) gas sorption measurements to investigate the specific surface area, pore volume, and size of Fe@AgW. The N_2 adsorption–desorption isotherm, pore size distribution curves, and BET surface area (Fig. 6) represented the surface area for Fe@AgW nanocomposite to be 39.543 m^2/g with an average pore volume of 0.057 cc/g. The large surface area and pore volume of the

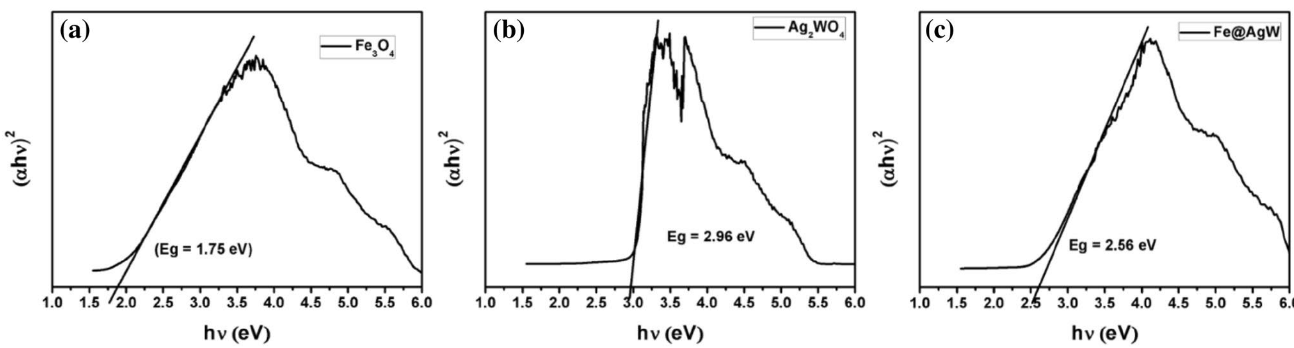

Fig. 5 Plot of transformed Kubelka–Munk function vs. the energy of light: **a** Fe_3O_4, **b** Ag_2WO_4, and **c** Fe@AgW nanocomposites

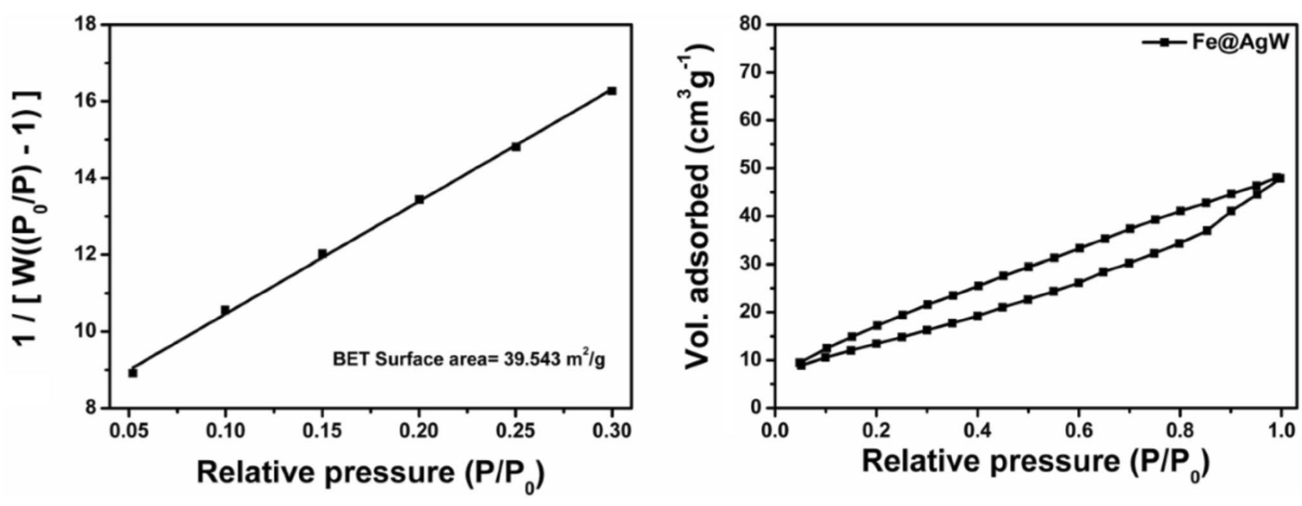

Fig. 6 N_2 adsorption–desorption isotherm of Fe@AgW nanocomposites

nanocomposite may provide more interfacial contact region for photo-induced charge transfer and apparently could be helpful in binding pollutants as well onto its surface, leading to faster photodegradation reaction (Li et al. 2014a, b; Lin et al. 2017; Rajamohan et al. 2017).

Photo-Fenton degradation of model dyes

Two model dyes (MB and MO) belonging to cationic and anionic classes were photo-degraded in the presence of nanocatalyst. For this, the characteristic absorption peaks of methyl orange (MO) at 464 nm and methylene blue (MB) at 664 nm were analyzed with the help of UV–Visible spectrophotometer at regular interval of time for both dyes after adding nanocomposite Fe@AgW and H_2O_2 in the reaction mixture under the influence of visible light. The degradation of both the dyes was negligible within 60 min in the absence of nanocatalyst, signifying their photo stabilities under visible light without any catalyst for 60 min (Fig. 7). It is important to mention that before starting the photo-Fenton procedure, the reaction mixtures were stirred under the dark condition to achieve adsorption–desorption equilibrium, and then degradation of dye was examined under visible light irradiation. The kinetic curves belonging to the degradation of MO and MB using a different precursor of catalysts are given in Fig. 6S and Fig. 7S (ESI). The degradation plots explicated that the degradation of both the dyes in the presence of AgW was lesser than Fe@AgW. However, the small decrease in the absorption of both the dyes in the presence of AgW and H_2O_2 advocates the formation of reactive species. MO was degraded 28% and 82% with AgW and Fe@AgW, respectively, for 120 min of irradiation time. On the other hand, MB was degraded 64% and 92% with AgW and Fe@AgW, respectively, for 60 min of irradiation time. This implies that the prepared nanocomposite has enhanced photocatalytic efficiency than its precursors. The significant enhancement in degradation also concludes the synergistic photo-Fenton process for degrading organic pollutants. The photocatalytic degradation kinetics was explored by

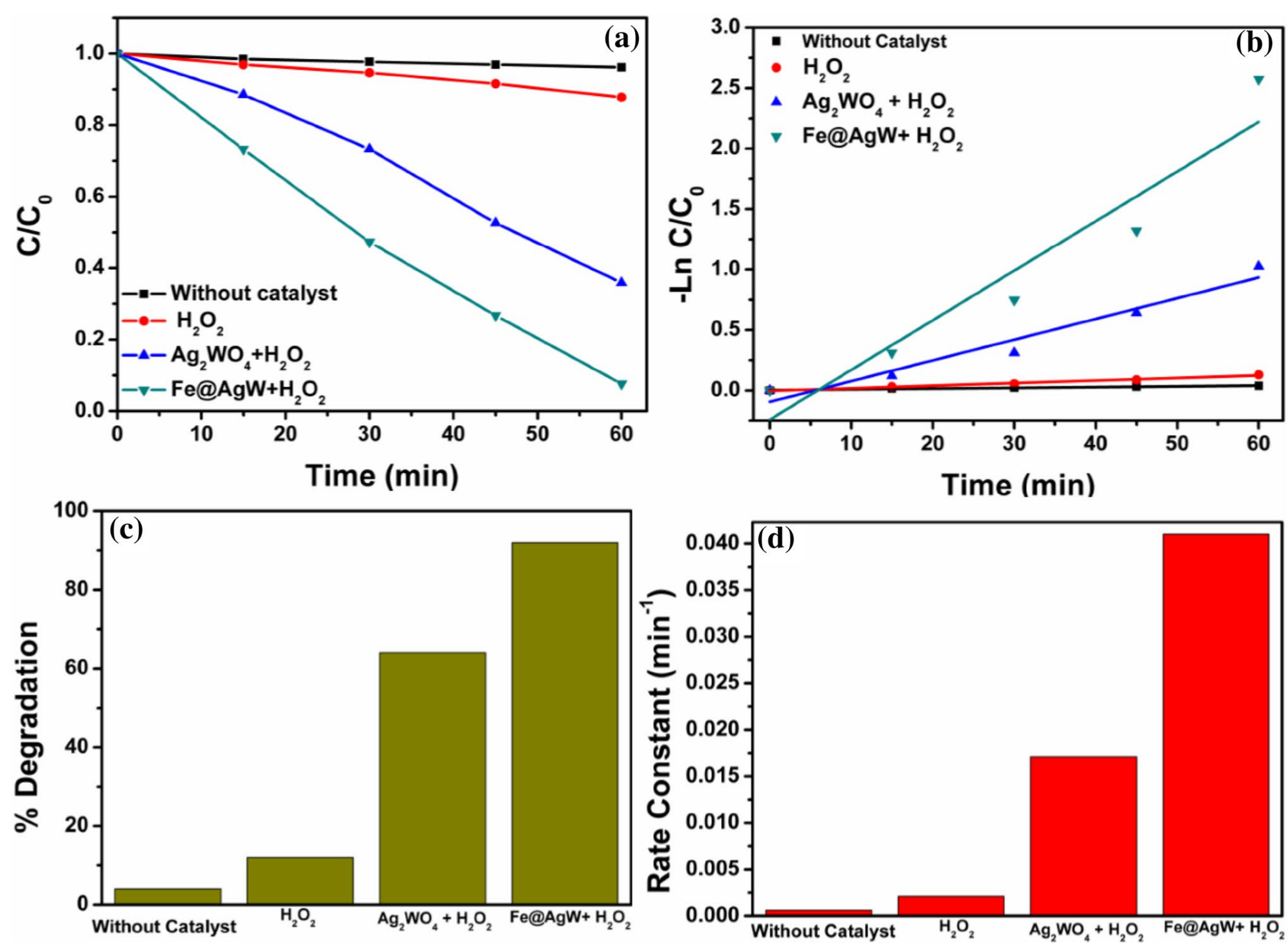

Fig. 7 **a**, **b** Kinetic curves for MB degradation under visible light irradiation, **c** The histogram shows the degradation rate and **d** histogram illustrates the values of rate constant for all the cases

applying pseudo-first-order kinetics by implying the Langmuir–Hinshelwood model equation:

$$\ln C/C_o = -kt,$$

where 'k' is the pseudo-first-order rate constant (min^{-1}), 't' is the irradiation time (min) 'C' is concentration, and 'C_o' is the initial concentration ($mg\ L^{-1}$) of dyes. The variations in (C/C_0) and − ln (C/C_0) as a function of irradiation time are given in Figs. 7 and 8, which showed a good linear relationship with the enhanced photocatalytic activity for Fe@AgW. The pseudo-first-order rate constant (k), the half-life of reaction ($t_{1/2}$), and linear regression coefficient (R^2) for all the catalysts are subsumed in Table 1S (ESI). The k value is high for Fe@AgW for both the dyes (0.0136 min^{-1} and 0.041 min^{-1}) and was highest as compared with AgW alone (0.0026 min^{-1} and 0.017 min^{-1}), which indicates the enhanced visible light efficacy of composite material. The SiO_2-coated magnetite, when combined with silver tungstate synergistically enhances the photocatalytic response under visible light irradiation by improving the charge separation at the heterojunction. The larger rate constant values for the final composite also advocate the homogeneous dispersion and availability of a larger number of active sites for degradation of pollutants (Li et al. 2014a, b). The histograms of degradation (%) and rate constants for different catalysts are illustrated in Figs. 7 and 8.

Degradation of bisphenol using Fe@AgW

To ensure the photo-Fenton process for the degradation of organic pollutants, the nanocomposites were also tested for degradation of bisphenol A (BPA), which is colorless water pollutants and eliminates any possibility of degradation due to photosensitization of dyes (Bandara et al. 1999). The degradation procedure was the same as for dyes

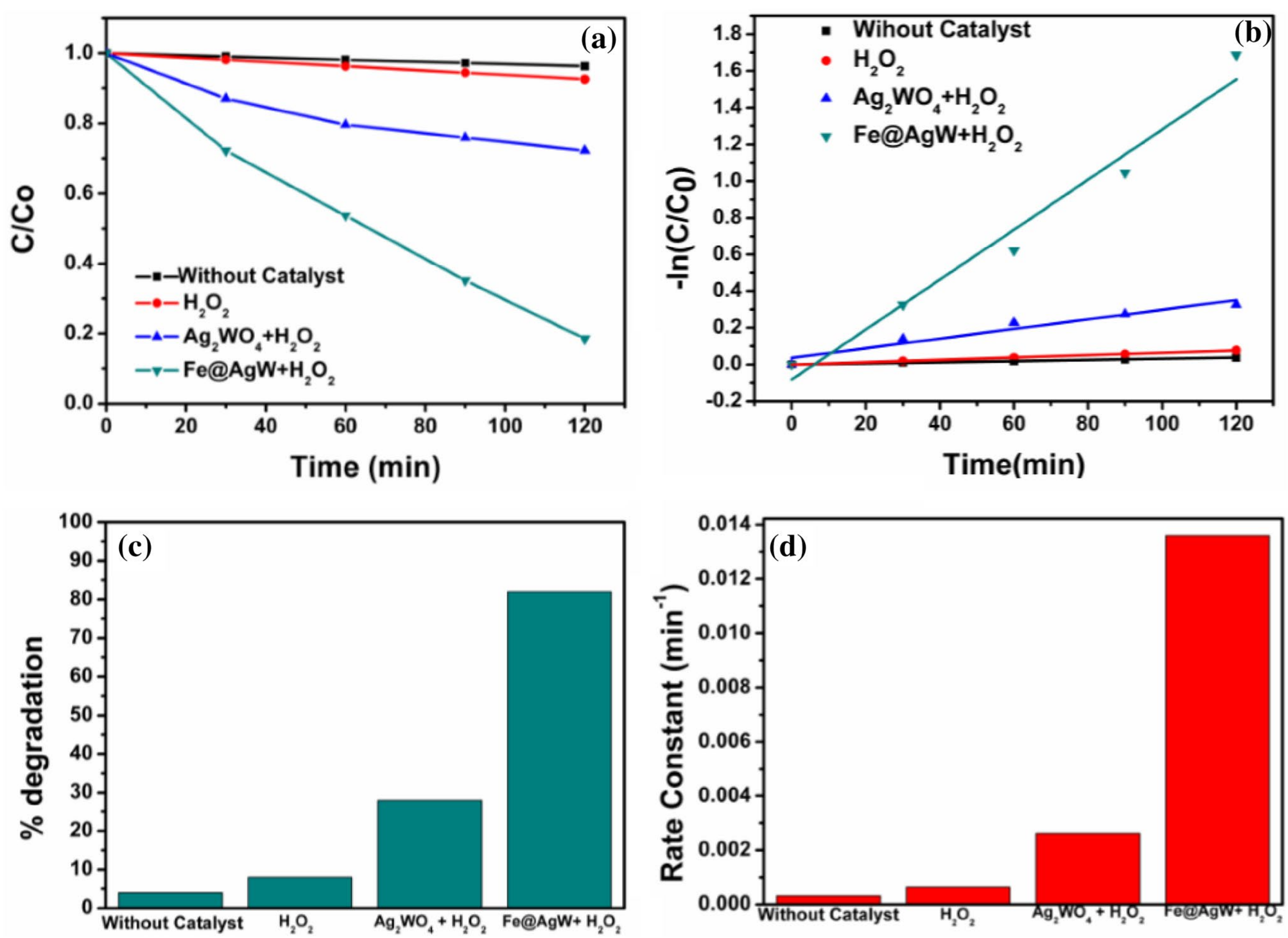

Fig. 8 **a**, **b** Kinetic curves for MO degradation under visible light irradiation, **c** The histogram shows the degradation rate and **d** histogram illustrates the values of rate constant for all the cases

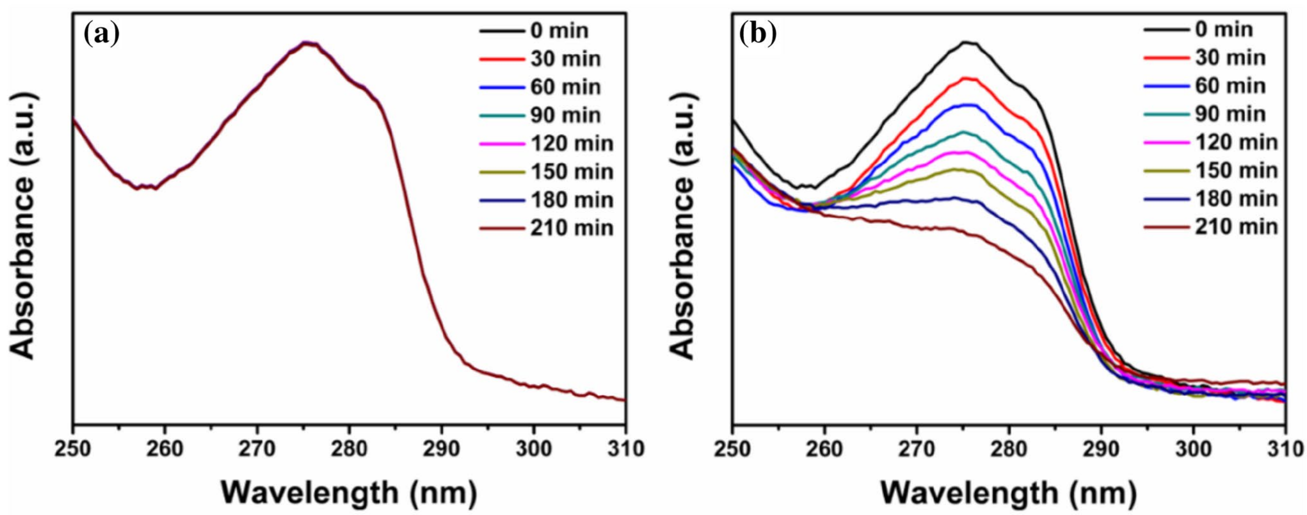

Fig. 9 Histogram showing treatment of BPA under **a** visible light irradiation without any catalyst. **b** Visible light irradiation in the presence of Fe@AgW catalyst and H_2O_2

and results are shown in Fig. 9 for visible light treatment with and without the use of catalyst.

Mechanism of photocatalytic activity

The excellent photo-induced degradation of model contaminants by Fe@AgW is believed to proceed through a photo-Fenton mechanism which operates under visible light. The degradation may take place through a series of chemical reactions, which includes the excitation of electrons from the valence band of silver tungstate to conduction band as band-gap is coherent to visible light, leaving the hole behind in valence band. The conduction (CB) and valence band (VB) edge potentials, E_{CB} and $E_{VB,}$ respectively, for Ag_2WO_4 and Fe_3O_4 were calculated from the following equations (a and b) (Morrison 1980):

$$E_{VB} = \chi - E_e + 0.5E_g, \tag{1a}$$

$$E_{CB} = E_{VB} - E_g, \tag{1b}$$

where χ is the electronegativity of the semiconductors, which can be calculated by the geometric mean of the absolute electronegativity of constituent atoms, E_e is the energy of free electrons on the hydrogen scale which is about 4.5 eV, and E_g is the bandgap of the respective semiconductor.

The calculated values of E_{CB} and E_{VB} for Ag_2WO_4 are − 0.064 and 3.03 eV, respectively. On the other hand, for Fe_3O_4, these are + 0.43 and + 2.86 eV. The conduction band of either of two species is not suitable for $^{\cdot}O_2^-$ generation as its potential value is less negative than the standard reduction potential value of − 0.33 eV for $O_2/^{\cdot}O_2^-$ generation. The valence band of Ag_2WO_4 lies more coherent with the standard reduction potential of $^{\cdot}OH$, H^+/H_2O (2.72 eV) (Zhu et al. 2017). Hence, organic pollutants can be easily degraded by the production of $^{\bullet}OH$ in photo-excited holes in VB of Ag_2WO_4. The photoexcited electrons, however, may pass to the magnetite nanosphere where $=Fe^{3+}$ conversion to $=Fe^{2+}$ occurs, which is the rate-determining step in Fenton's process, where, $=Fe^{3+}$ and $=Fe^{2+}$ species are active sites at solid–liquid interfaces of heterogeneous Fenton's reactions. The degradation of organic pollutants is mainly attributed to the formation of $^{\cdot}OH$ radicals at solid–liquid interfaces of nanocomposites due to the catalyzed decomposition of H_2O_2 (Zubir et al. 2014).

The various photochemical reaction may occur on the solid–liquid junction of two semiconductors' nanocomposites with the illumination of visible light, and there is excitation of electrons to the conduction band of Ag_2WO_4 to nanosphere of Fe_3O_4 where the electron transfer between $=Fe^{3+}$ and $=Fe^{2+}$ was escalated and, consequently, increasing the production of $^{\cdot}OH$ (Liu et al. 2018; Zhang et al. 2016a, b, c). The reaction shown in Eqs. (2–5) represents the generation of $^{\cdot}OH$ at the heterogeneous surface of composite, overcoming the limitations of homogeneous Fenton's processes (Luo et al. 2010; Wang et al. 2010). The $=Fe$ (IV) species shown in Eq. (8) may also produce in solution, but they have a lesser impact on organics in comparison with $^{\cdot}OH$ (Keenan and Sedlak 2008). Visible light illumination leads to the excitation of electrons in metal oxide semiconductor materials (Eq. 6, 7) and these heterogeneous semiconductors synergistically contribute to the degradation of organic pollutants in water through production of $^{\cdot}OH$ in conduction band through electron transfer and in valence band through holes generation with prolonged electron–hole recombination process by transferring electrons to Fe^{2+}/Fe^{3+} redox couple (Ojha et al. 2017).

$$Fe^{2+} + H_2O_2 \rightarrow +Fe^{3+} +^{\cdot} OH + OH^{-}, \quad (2)$$

$$Fe^{3+} + H_2O_2 \rightarrow Fe^{2+} + HO_2^{\cdot} + H^{+}, \quad (3)$$

$$Fe^{2+} + HO_2^{\cdot} + H^{+} \rightarrow Fe^{3+} + H_2O_2, \quad (4)$$

$$Fe^{3+} + HO_2^{\cdot} \rightarrow Fe^{2+} + O_2 + H^{+}, \quad (5)$$

$$\text{Fe oxide} + hv \rightarrow \text{Fe oxide} (e^{-} + h^{+}), \quad (6)$$

$$Ag_2WO_4 + hv \rightarrow Ag_2WO_4(e^{-} + h^{+}), \quad (7)$$

$$Fe^{3+} + hv + Ag_2WO_4 \rightarrow O = Fe(IV) + Ag_2WO_4(e^{-}) \quad (8)$$

$$\text{Fe oxide} + Ag_2WO_4 \rightarrow O = \text{Fe oxide} (e^{-}) + Ag_2WO_4, \quad (9)$$

$$\text{Fe oxide} (e^{-}) + = Fe^{3+} \rightarrow +\text{Fe oxide} + = Fe^{2+}. \quad (10)$$

The plausible mechanism of photo-Fenton catalytic degradation of model pollutants through synergic Fe@AgW nanocomposite in the presence of visible light has been demonstrated in Fig. 10.

To support the findings, the active species produced during the reaction were trapped using different scavengers. For this purpose, isopropanol (IPA) was used as hydroxyl radical ($^{\cdot}OH$) and triethanolamine (TEA) was used for holes (h^+) scavenging. The use of benzoquinone (BQ) was also tested for quenching superoxide ion radical (O_2^{-*}) (Devi et al. 2009; Maezono et al. 2011; Mehrvar et al. 2001). The results are represented in Fig. 11a and are in better agreement with the proposed mechanism. The reaction conditions for testing the impact of scavenger on the photo-Fenton catalytic process were kept constant and it was observed that the degradation of model dye MB was decreased to 31% when IPA was used as a scavenger for ·OH. The degradation efficiency was decreased to 46% when TEA was used as a scavenger. The results were in accordance with the proposed mechanism as there was a lesser decrease in degradation of MB dye with Fe@AgW catalyst when BQ was used as a scavenger. This indicates that the decrease in degradation with BQ was least which is attributed to the minimal production of superoxide ion radical during photo-Fenton reaction.

Recycling and reusability

The recycling and reusability of the catalyst are some of the crucial factors for ensuring field application. The reusability of Fe@AgW was investigated for four recycles of photo-Fenton's degradation of MB dye. The results are represented in Fig. 11b. After each catalytic recycle, the catalyst was recovered and washed to remove any residual content. The catalyst was finally dried before using it for the next cycle. Figure 12 shows the MB solution before treatment and after treatment using nanocomposite which can be easily removed

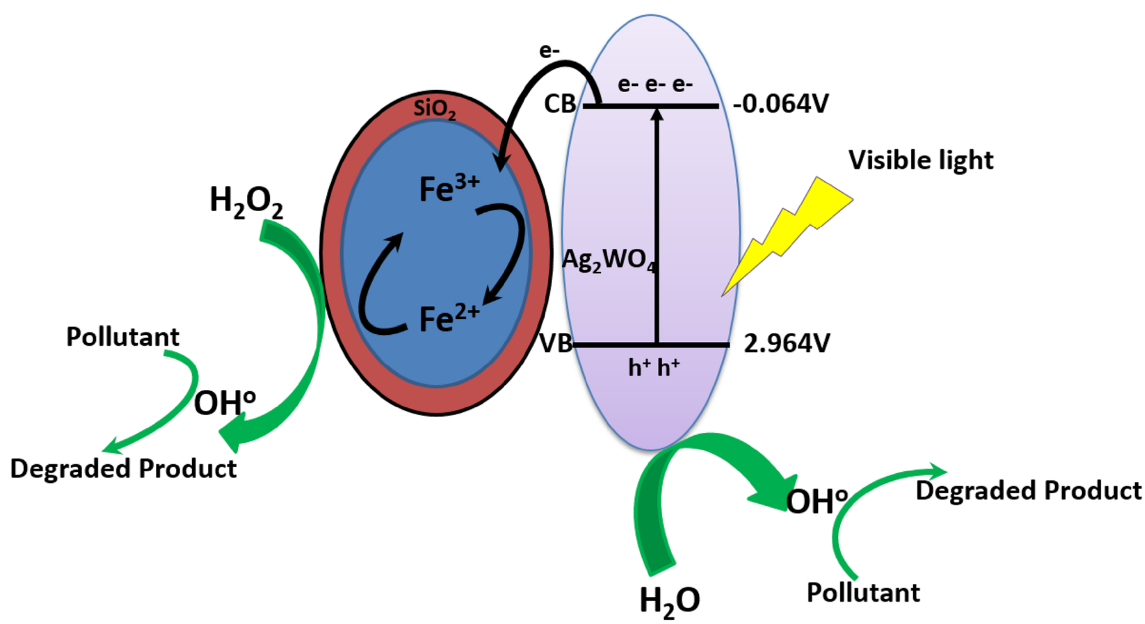

Fig. 10 Proposed mechanism for visible light-assisted photo-Fenton catalytic mechanism for Fe@AgW nanocomposite

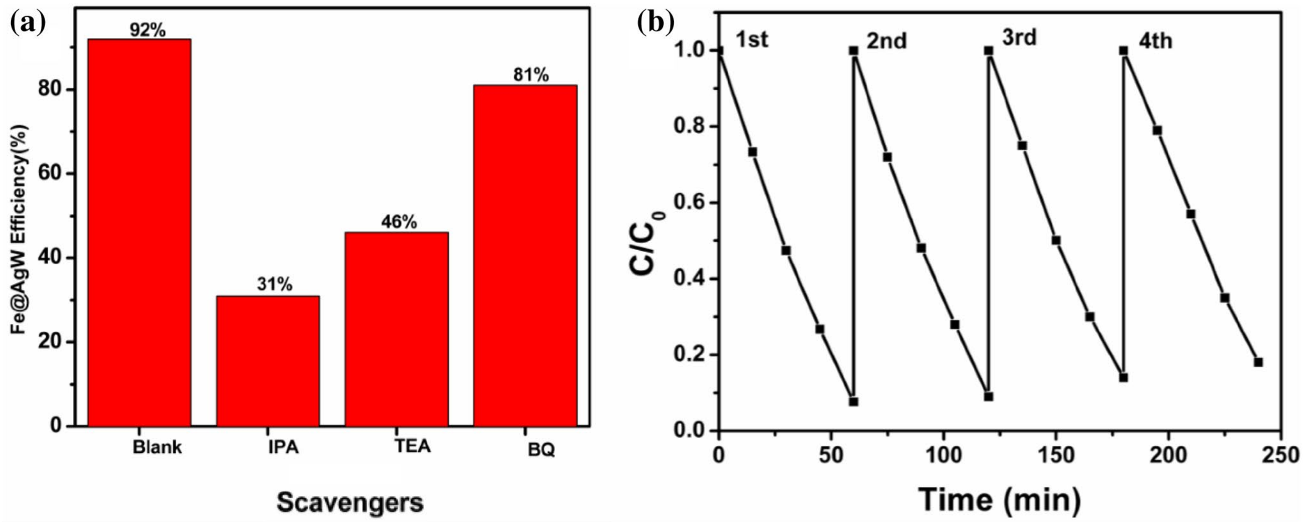

Fig. 11 **a** Histogram showing the impact of scavengers on the photo-Fenton catalytic activity of Fe@AgW nanocomposite, **b** recyclability of Fe@AgW nanocomposite for photo-Fenton catalytic degradation of MB dye

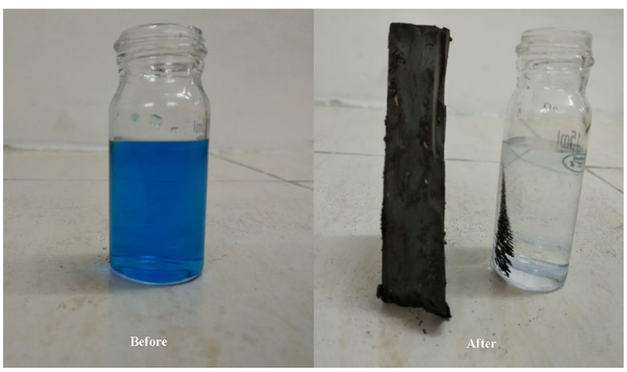

Fig. 12 The solution of MB dye before and after treatment using Fe@AgW

using external magnet. The experimental conditions have remained the same for each cycle, and the figure shows no significant change even after four cycles.

Antibacterial activities of nanocomposite

To find out the effectiveness of photocatalyst and its extended use for wastewater treatment in terms of biological contamination, the catalyst was tested against selected bacterial strains under controlled conditions. Four bacterial strains, *K. pneumoniae*, *S. aureus*, *P. aeruginosa* and *B. subtilis*, were selected belonging to the Gram-positive and Gram-negative category. Magnetite nanomaterials have been reported to be effective against pathogenic microorganisms (Chen et al. 2008; Prucek et al. 2011), and the antibacterial activities of silver tungstate nanoparticles

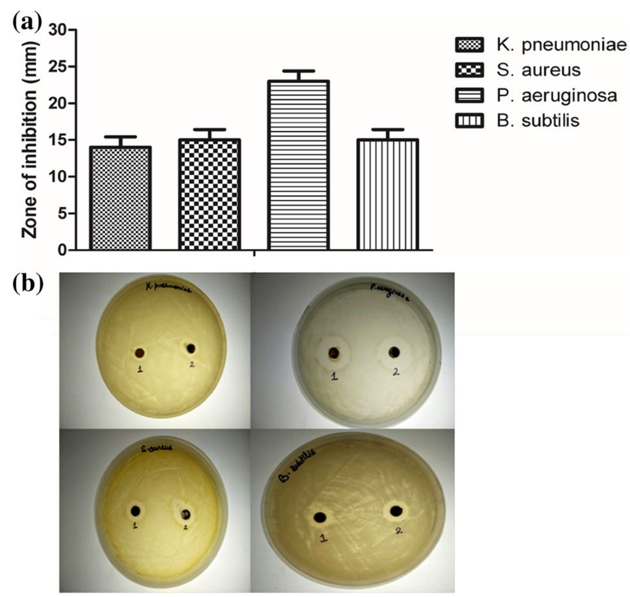

Fig. 13 Antibacterial studies of Fe@AgW nanocomposites. **a** Histogram illustrating the respective zone of inhibition for different bacterial strains; **b** pictorial presentation of the zone of inhibition for K. *pneumoniae*, S. *aureus*, P. *aeruginosa* and B. *subtilis*

have also been explored (Ali et al. 2016; Assis et al. 2018; Dutta et al. 2014). Herein, we examined the antibacterial

Table 1 MIC and MBC of Fe@AgW nanocomposite

	K. pneumoniae	*S. aureus*	*P. aeruginosa*	*B. subtilis*
MIC	0.9	0.9	0.46	0.9
MBC	1.8	1.8	0.9	1.8

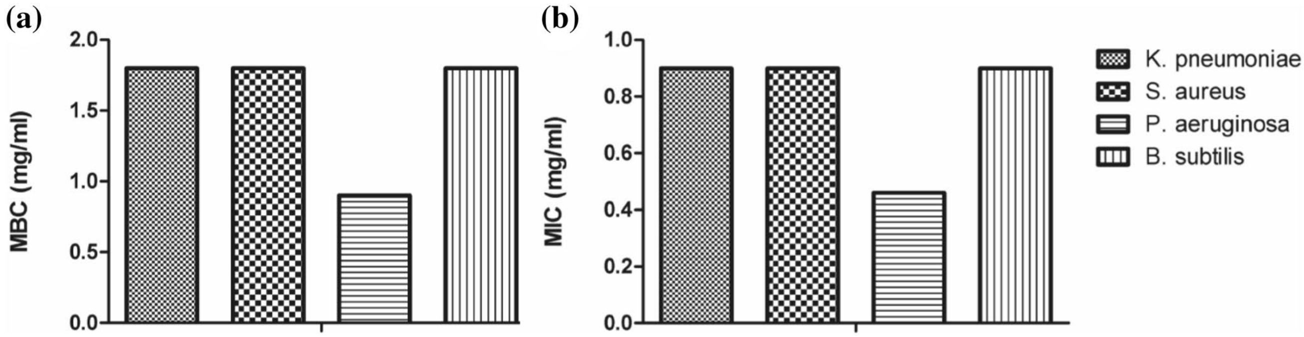

Fig. 14 **a** Minimum bacterial concentration (MBC) of Fe@AgW and **b** minimum inhibition concentration (MIC) of Fe@AgW

activity of silver tungstate-modified magnetite nanomaterials (Fe@AgW).

Agar well diffusion assay

Agar well diffusion assay showed the potent antibacterial activity of nanocomposite (Fe@AgW) against Gram-positive as well as Gram-negative pathogenic microorganisms. As shown in Fig. 13a, *P. aeruginosa* showed maximum susceptibility to nanocomposite, whereas other microorganisms showed moderate activity. Figure 13b represents the bactericidal properties, which can be attributed to the activity of nanocomposite in visible light. The photoelectron was generated in the conduction band and transferred to the surface of nanocomposites for generating radicals. The formation of reactive oxygenated species in the photocatalytic procedure further creates oxidative stress to the cells and ultimately leads to the inactivation of pathogenic stains (Khan et al. 2017). However, the zone of inhibition was not dependent on cell wall composition of microorganisms as it showed differential activity in Gram-negative tested microorganisms as shown in Fig. 13b.

Minimum bacterial concentration (MBC) and minimum inhibition concentration (MIC)

The MBC of nanocomposite (Fe@AgW) was found to be in range of 0.9–1.8 mg/ml and MIC was observed to be in the range of 0.46–0.9 mg/ml for four tested microorganisms which confirmed the antibacterial potential of nanocomposites (Table 1). The MBC and MIC of the nanocomposite for four tested microorganisms are shown in Fig. 14.

Conclusion

We reported the facile synthesis of silver tungstate-modified magnetite nanomaterials by the sonochemical method—the silica-coated magnetite nanoparticles were coupled with silver tungstate where coating prevents agglomeration of nanoparticles in solution. UV-DRS studies of nanocomposite demonstrated the bandgap potentials of semiconductor material and also XRD analysis confirms the strong interaction of magnetite and silver tungstate. The nanocomposite was successfully demonstrated to act against model dyes (MB and MO), colorless organic pollutant (BPA), and pathogenic bacterial strains that contaminate water. A synergistic electron transfer to Fe^{3+}/Fe^{2+} redox couple and a plausible photo-Fenton mechanism has been proposed for the catalytic activity of nanocomposite. The recyclability, easy magnetic recovery, diversified use of catalyst, and visible light active nanocatalyst are indispensable for its large-scale use.

Acknowledgments P.K. is thankful to the Science and Engineering Research Board (SERB), DST, India (Project File no. ECR/2015/000541) for the research funding. The authors are grateful to the Department of Chemistry, University of Delhi and USIC, University of Delhi, New Delhi, for characterization data. The authors acknowledge Deshbandhu College for providing the facility for the research work and the Department of biotechnology, Punjab University, Chandigarh, India for antibacterial activity.

Compliance with ethical standards

Conflict of interest There is no conflict of interest.

References

Abou-Elela SI, Hellal MS, Aly OH, Abo-Elenin SA (2017) Decentralized wastewater treatment using passively aerated biological filter. Environ Technol. https://doi.org/10.1080/09593330.2017.1385648

Ali ZA, Yahya R, Sekaran SD, Puteh R (2016) Green synthesis of silver nanoparticles using apple extract and its antibacterial properties. Adv Mater Sci Eng

Assis M, Cordoncillo E, Torres-Mendieta R, Beltrán-Mir H, Mínguez-Vega G, Oliveira R, Longo E (2018) Towards the scale-up of the formation of nanoparticles on α-Ag 2 WO 4 with bactericidal properties by femtosecond laser irradiation. Sci Rep 8(1):1884

Atla SB, Lin W-R, Chien T-C, Tseng M-J, Shu J-C, Chen C-C, Chen C-Y (2018) Fabrication of Fe_3O_4/ZnO magnetite core shell and its application in photocatalysis using sunlight. Mater Chem Phys 216:380–386. https://doi.org/10.1016/j.matchemphys.2018.06.020

Balouiri M, Sadiki M, Ibnsouda SK (2016) Methods for in vitro evaluating antimicrobial activity: a review. J Pharm Anal 6(2):71–79. https://doi.org/10.1016/j.jpha.2015.11.005

Bandara J, Mielczarski J, Kiwi J (1999) Photosensitized degradation of azo dyes on Fe, Ti, and Al oxides. Mechanism of charge transfer during the degradation. Langmuir 15(22):7680–7687

Bokare AD, Choi W (2014) Review of iron-free Fenton-like systems for activating H2O2 in advanced oxidation processes. J Hazard Mater 275:121–135. https://doi.org/10.1016/j.jhazmat.2014.04.054

Boyer C, Whittaker MR, Bulmus V, Liu J, Davis TP (2010) The design and utility of polymer-stabilized iron-oxide nanoparticles for nanomedicine applications. Npg Asia Materials 2:23. https://doi.org/10.1038/asiamat.2010.6

Chen H, Xu Y (2014) Photoactivity and stability of Ag_2WO_4 for organic degradation in aqueous suspensions. Appl Surf Sci 319:319–323. https://doi.org/10.1016/j.apsusc.2014.05.115

Chen W-J, Tsai P-J, Chen Y-C (2008) Functional Fe_3O_4/TiO_2 core/shell magnetic nanoparticles as photokilling agents for pathogenic bacteria. Small 4(4):485–491. https://doi.org/10.1002/smll.200701164

Crini G, Lichtfouse E, Wilson LD, Morin-Crini N (2018) Conventional and non-conventional adsorbents for wastewater treatment. Environ Chem Lett. https://doi.org/10.1007/s10311-018-0786-8

Cui J, Zhang Z, Jiang H, Liu D, Zou L, Guo X Guo D (2019) Ultrahigh recovery of fracture strength on mismatched fractured amorphous surfaces of silicon carbide. ACS Nano

Cui J, Zhang Z, Liu D, Zhang D, Hu W, Zou L, Tang C (2019b) Unprecedented piezoresistance coefficient in strained silicon carbide. Nano Lett 19(9):6569–6576

Devi LG, Kumar SG, Reddy KM, Munikrishnappa C (2009) Photo degradation of Methyl orange an azo dye by advanced fenton process using zero valent metallic iron: influence of various reaction parameters and its degradation mechanism. J Hazard Mater 164(2–3):459–467

Di L, Yang H, Xian T, Liu X, Chen X (2019) Photocatalytic and photo-fenton catalytic degradation activities of Z-scheme $Ag_2S/BiFeO_3$ heterojunction composites under visible-light irradiation. Nanomaterials 9(3):399

Dickhout JM, Moreno J, Biesheuvel PM, Boels L, Lammertink RGH, de Vos WM (2017) Produced water treatment by membranes: a review from a colloidal perspective. J Colloid Interface Sci 487:523–534. https://doi.org/10.1016/j.jcis.2016.10.013

Du W, Xu Q, Jin D, Wang X, Shu Y, Kong L, Hu X (2018) Visible-light-induced photo-Fenton process for the facile degradation of metronidazole by Fe/Si codoped TiO_2. RSC Adv 8(70):40022–40034. https://doi.org/10.1039/C8RA08114J

Dutta DP, Singh A, Ballal A, Tyagi AK (2014) High adsorption capacity for cationic dye removal and antibacterial properties of sonochemically synthesized Ag_2WO_4 nanorods. Eur J Inorg Chem 2014(33):5724–5732

Emmert EAB, Handelsman J (1999) Biocontrol of plant disease: a (Gram−) positive perspective. FEMS Microbiol Lett 171(1):1–9. https://doi.org/10.1111/j.1574-6968.1999.tb13405.x

Fakhri A, Naji M, Nejad PA (2017) Adsorption and photocatalysis efficiency of magnetite quantum dots anchored tin dioxide nanofibers for removal of mutagenic compound: toxicity evaluation and antibacterial activity. J Photochem Photobiol, B 173:204–209. https://doi.org/10.1016/j.jphotobiol.2017.05.041

Fan FL, Qin Z, Bai J, Rong WD, Fan FY, Tian W, Zhao L (2012) Rapid removal of uranium from aqueous solutions using magnetic $Fe_3O_4@SiO_2$ composite particles. J Environ Radioact 106:40–46

Fisher P (1999) Review of using rhodamine b as a marker for wildlife studies. Wildlife Society Bull (1973–2006) 27(2):318–329

Garg VK, Amita M, Kumar R, Gupta R (2004) Basic dye (methylene blue) removal from simulated wastewater by adsorption using Indian Rosewood sawdust: a timber industry waste. Dyes Pigm 63(3):243–250. https://doi.org/10.1016/j.dyepig.2004.03.005

Gjipalaj J, Alessandri I (2017) Easy recovery, mechanical stability, enhanced adsorption capacity and recyclability of alginate-based TiO_2 macrobead photocatalysts for water treatment. J Environ Chem Eng 5(2):1763–1770. https://doi.org/10.1016/j.jece.2017.03.017

Gopakumar DA, Pasquini D, Henrique MA, de Morais LC, Grohens Y, Thomas S (2017) Meldrum's acid modified cellulose nanofiber-based polyvinylidene fluoride microfiltration membrane for dye water treatment and nanoparticle removal. ACS Sustain Chem Eng 5(2):2026–2033. https://doi.org/10.1021/acssuschemeng.6b02952

Guo X, Mao F, Wang W, Yang Y, Bai Z (2015) Sulfhydryl-modified Fe_3O_4@ SiO_2 core/shell nanocomposite: synthesis and toxicity assessment in vitro. ACS Appl Mater Interfaces 7(27):14983–14991

Hongping H, Zhong Y, Liang X, Wei T, Jianxi Z, Wang CY (2015) Natural magnetite: an efficient catalyst for the degradation of organic contaminant. Sci Rep 5:10139

Keenan CR, Sedlak DL (2008) Factors affecting the yield of oxidants from the reaction of nanoparticulate zero-valent iron and oxygen. Environ Sci Technol 42(4):1262–1267. https://doi.org/10.1021/es7025664

Khan S, Runguo W, Tahir K, Jichuan Z, Zhang L (2017) Catalytic reduction of 4-nitrophenol and photo inhibition of Pseudomonas aeruginosa using gold nanoparticles as photocatalyst. J Photochem Photobiol, B 170:181–187. https://doi.org/10.1016/j.jphotobiol.2017.04.006

Kumari P, Parashara H (2018) β-cyclodextrin modified magnetite nanoparticles for efficient removal of eosin and phloxine dyes from aqueous solution. Mater Today Proc 5(7):15473–15480

Kumari P, Gautam R, Yadav H, Kushwaha V, Mishra A, Gupta S, Arora V (2016) Efficient reduction of C–N multiple bonds catalyzed by magnetically retrievable magnetite nanoparticles with sodium borohydride. Catal Lett 146(10):2149–2156

Kumari P, Kumar S, Gupta S, Mishra A, Kumar A (2018) Efficacious and selective oxidation of atrazine with hydrogen peroxide catalyzed by magnetite nanoparticles: influence of reaction media. ChemistrySelect 3(7):2135–2139

Kumari P, Kumar S, Nisa K, Sharma DK (2019) Efficient system for encapsulation and removal of paraquat and diquat from aqueous solution: 4-sulfonatocalix [n] arenes and its magnetite modified nanomaterials. J Environ Chem Eng 103130

Kummu M, Guillaume JHA, de Moel H, Eisner S, Flörke M, Porkka M, Ward PJ (2016) The world's road to water scarcity: shortage and stress in the 20th century and pathways towards sustainability. Sci Rep 6:38495. https://doi.org/10.1038/srep38495

Li X, Kolltveit KM, Tronstad L, Olsen I (2000) Systemic diseases caused by oral infection. Clin Microbiol Rev 13(4):547–558

Li G, Wang Y, Mao L (2014a) Recent progress in highly efficient Ag-based visible-light photocatalysts. RSC Adv 4(96):53649–53661. https://doi.org/10.1039/C4RA08044K

Li X, Liu D, Song S, Zhang H (2014b) $Fe_3O_4@SiO_2@TiO_2@Pt$ hierarchical core-shell microspheres: controlled synthesis, enhanced degradation system, and rapid magnetic separation to recycle. Cryst Growth Des 14(11):5506–5511. https://doi.org/10.1021/cg501164c

Lin M, Gao Y, Diefenbach TJ, Shen JK, Hornicek FJ, Park YI, Duan Z (2017) Facial layer-by-layer engineering of upconversion nanoparticles for gene delivery: near-infrared-initiated fluorescence resonance energy transfer tracking and overcoming drug resistance in ovarian cancer. ACS Appl Mater Interfaces 9(9):7941–7949

Liu R, Xu Y, Chen B (2018) Self-assembled nano-FeO (OH)/reduced graphene oxide aerogel as a reusable catalyst for photo-Fenton degradation of phenolic organics. Environ Sci Technol 52(12):7043–7053. https://doi.org/10.1021/acs.est.8b01043

Luo W, Zhu L, Wang N, Tang H, Cao M, She Y (2010) Efficient removal of organic pollutants with magnetic nanoscaled $BiFeO_3$ as a reusable heterogeneous Fenton-like catalyst. Environ Sci Technol 44(5):1786–1791

Luo W, Phan HV, Xie M, Hai FI, Price WE, Elimelech M, Nghiem LD (2017) Osmotic versus conventional membrane bioreactors integrated with reverse osmosis for water reuse: biological stability, membrane fouling, and contaminant removal. Water Res 109:122–134. https://doi.org/10.1016/j.watres.2016.11.036

Maezono T, Tokumura M, Sekine M, Kawase Y (2011) Hydroxyl radical concentration profile in photo-Fenton oxidation process: generation and consumption of hydroxyl radicals during the discoloration of azo-dye Orange II. Chemosphere 82(10):1422–1430

Manikandan A, Vijaya JJ, Mary JA, Kennedy LJ, Dinesh A (2014) Structural, optical and magnetic properties of Fe_3O_4 nanoparticles prepared by a facile microwave combustion method. J Ind Eng Chem 20(4):2077–2085. https://doi.org/10.1016/j.jiec.2013.09.035

Mehrvar M, Anderson WA, Moo-Young M (2001) Photocatalytic degradation of aqueous organic solvents in the presence of hydroxyl radical scavengers. Int J Photoenergy 3(4):187–191

Michałowicz J (2014) Bisphenol A—sources, toxicity and biotransformation. Environ Toxicol Pharmacol 37(2):738–758. https://doi.org/10.1016/j.etap.2014.02.003

Mishra P, Patnaik S, Parida K (2019) An overview of recent progress on noble metal modified magnetic Fe_3O_4 for photocatalytic pollutant degradation and H2 evolution. Catal Sci Technol 9(4):916–941. https://doi.org/10.1039/C8CY02462F

Morrison SR (1980) Electrochemistry at semiconductor and oxidized metal electrodes

Ojha DP, Joshi MK, Kim H (2017) Photo-Fenton degradation of organic pollutants using a zinc oxide decorated iron oxide/reduced graphene oxide nanocomposite. Ceram Int 43(1, Part B):1290–1297. https://doi.org/10.1016/j.ceramint.2016.10.079

Olliver JR, Wild CP, Sahay P, Dexter S, Hardie LJ (2003) Chromoendoscopy with methylene blue and associated DNA damage in Barrett's oesophagus. Lancet 362(9381):373–374. https://doi.org/10.1016/S0140-6736(03)14026-3

Pastrana-Martínez LM, Pereira N, Lima R, Faria JL, Gomes HT, Silva AMT (2015) Degradation of diphenhydramine by photo-Fenton using magnetically recoverable iron oxide nanoparticles as catalyst. Chem Eng J 261:45–52. https://doi.org/10.1016/j.cej.2014.04.117

Pirkanniemi K, Sillanpää M (2002) Heterogeneous water phase catalysis as an environmental application: a review. Chemosphere 48(10):1047–1060. https://doi.org/10.1016/S0045-6535(02)00168-6

Prucek R, Tuček J, Kilianová M, Panáček A, Kvítek L, Filip J, Zbořil R (2011) The targeted antibacterial and antifungal properties of magnetic nanocomposite of iron oxide and silver nanoparticles. Biomaterials 32(21):4704–4713

Rajamohan S, Kumaravel V, Muthuramalingam R, Ayyadurai S, Abdel-Wahab A, Sub Kwak B, Sreekantan S (2017) Fe_3O_4–Ag_2WO_4: facile synthesis, characterization and visible light assisted photocatalytic activity. New J Chem 41(20):11722–11730. https://doi.org/10.1039/C7NJ03004E

Ramírez LP, Landfester K (2003) Magnetic Polystyrene Nanoparticles with a High Magnetite Content Obtained by Miniemulsion Processes. Macromol Chem Phys 204(1):22–31. https://doi.org/10.1002/macp.200290052

Sagapuram D, Yeung H, Guo Y, Mahato A, M'Saoubi R, Compton WD, Chandrasekar S (2015) On control of flow instabilities in cutting of metals. CIRP Ann 64(1):49–52

Särkkä H, Bhatnagar A, Sillanpää M (2015) Recent developments of electro-oxidation in water treatment—a review. J Electroanal Chem 754:46–56. https://doi.org/10.1016/j.jelechem.2015.06.016

Shekofteh-Gohari M, Habibi-Yangjeh A (2015) Ternary ZnO/Ag3VO4/Fe3O4 nanocomposites: novel magnetically separable photocatalyst for efficiently degradation of dye pollutants under visible-light irradiation. Solid State Sci 48:177–185. https://doi.org/10.1016/j.solidstatesciences.2015.08.010

Singh S, Mahalingam H, Singh PK (2013) Polymer-supported titanium dioxide photocatalysts for environmental remediation: a review. Appl Catal A 462–463:178–195. https://doi.org/10.1016/j.apcata.2013.04.039

Soon AN, Hameed B (2011) Heterogeneous catalytic treatment of synthetic dyes in aqueous media using Fenton and photo-assisted Fenton process. Desalination 269(1–3):1–16

Srikanth B, Goutham R, Badri Narayan R, Ramprasath A, Gopinath KP, Sankaranarayanan AR (2017) Recent advancements in supporting materials for immobilised photocatalytic applications in waste water treatment. J Environ Manage 200:60–78. https://doi.org/10.1016/j.jenvman.2017.05.063

Tatoulis T, Stefanakis A, Frontistis Z, Akratos CS, Tekerlekopoulou AG, Mantzavinos D, Vayenas DV (2017) Treatment of table olive washing water using trickling filters, constructed wetlands and electrooxidation. Environ Sci Pollut Res 24(2):1085–1092. https://doi.org/10.1007/s11356-016-7058-6

Thune RL, Stanley LA, Cooper RK (1993) Pathogenesis of gram-negative bacterial infections in warmwater fish. Annu Rev Fish Dis 3:37–68. https://doi.org/10.1016/0959-8030(93)90028-A

Van Den Berg AJ, Juffermans CAH (1982) The polymorphism of silver tungstate Ag_2WO_4. J Appl Crystallogr 15(1):114–116. https://doi.org/10.1107/S0021889882011510

Vutskits L, Briner A, Klauser P, Gascon E, Dayer AG, Kiss JZ, Muller D, Licker MJ, Morel DR (2008) Adverse effects of methylene blue on the central nervous system. Anesthesiol J Am Soc Anesthesiol 108(4):684–692. https://doi.org/10.1097/aln.0b013e3181684be4

Wang N, Zhu L, Wang M, Wang D, Tang H (2010) Sono-enhanced degradation of dye pollutants with the use of H2O2 activated by Fe3O4 magnetic nanoparticles as peroxidase mimetic. Ultrason Sonochem 17(1):78–83. https://doi.org/10.1016/j.ultsonch.2009.06.014

Wang W, Mao Q, He H, Zhou M (2013) Fe_3O_4 nanoparticles as an efficient heterogeneous Fenton catalyst for phenol removal at relatively wide pH values. Water Sci Technol 68(11):2367–2373

Wang B, Zhang Z, Chang K, Cui J, Rosenkranz A, Yu J, Luo J (2018a) New deformation-induced nanostructure in silicon. Nano Lett 18(7):4611–4617

Wang Q, Xu P, Zhang G, Zhang W, Hu L, Wang P (2018b) Characterization of visible-light photo-Fenton reactions using Fe-doped ZnS (Fex-ZnS) mesoporous microspheres. Phys Chem Chem Phys 20(27):18601–18609. https://doi.org/10.1039/C8CP02609B

Xie S, Huang P, Kruzic JJ, Zeng X, Qian H (2016) A highly efficient degradation mechanism of methyl orange using Fe-based metallic glass powders. Sci Rep 6:21947. https://doi.org/10.1038/srep21947

Xuefei W, Can F, Ping W, Huogen Y, Jiaguo Y (2013) Hierarchically porous metastable β-Ag_2WO_4 hollow nanospheres: controlled synthesis and high photocatalytic activity. Nanotechnology 24(16):165602

Yang S-T, Zhang W, Xie J, Liao R, Zhang X, Yu B, Guo Z (2015) Fe_3O_4@ SiO_2 nanoparticles as a high-performance Fenton-like catalyst in a neutral environment. RSC Adv 5(7):5458–5463

Zhang R, Cui H, Yang X, Tang H, Liu H, Li Y (2012a) Facile hydrothermal synthesis and photocatalytic activity of rod-like nanosized silver tungstate. Micro Nano Lett 7(12):1285–1288. https://doi.org/10.1049/mnl.2012.0765

Zhang Z, Huo F, Zhang X, Guo D (2012b) Fabrication and size prediction of crystalline nanoparticles of silicon induced by nanogrinding with ultrafine diamond grits. Scripta Mater 67(7–8):657–660

Zhang Z, Song Y, Xu C, Guo D (2012c) A novel model for undeformed nanometer chips of soft-brittle HgCdTe films induced by ultrafine diamond grits. Scripta Mater 67(2):197–200

Zhang Z, Huo Y, Guo D (2013) A model for nanogrinding based on direct evidence of ground chips of silicon wafers. Sci China Technol Sci 56(9):2099–2108

Zhang Z, Guo D, Wang B, Kang R, Zhang B (2015) A novel approach of high speed scratching on silicon wafers at nanoscale depths of cut. Sci Rep 5:16395

Zhang J, Zhang X, Wang Y (2016a) Degradation of phenol by a heterogeneous photo-Fenton process using Fe/Cu/Al catalysts. RSC Adv 6(16):13168–13176. https://doi.org/10.1039/C5RA20897A

Zhang Z, Wang B, Zhou P, Guo D, Kang R, Zhang B (2016b) A novel approach of chemical mechanical polishing using environment-friendly slurry for mercury cadmium telluride semiconductors. Sci Rep 6:22466

Zhang Z, Wang B, Zhou P, Kang R, Zhang B, Guo D (2016c) A novel approach of chemical mechanical polishing for cadmium zinc telluride wafers. Sci Rep 6:26891

Zhang Z, Cui J, Wang B, Wang Z, Kang R, Guo D (2017) A novel approach of mechanical chemical grinding. J Alloy Compd 726:514–524

Zhang Z, Shi Z, Du Y, Yu Z, Guo L, Guo D (2018) A novel approach of chemical mechanical polishing for a titanium alloy using an environment-friendly slurry. Appl Surf Sci 427:409–415

Zhang Z, Cui J, Zhang J, Liu D, Yu Z, Guo D (2019) Environment friendly chemical mechanical polishing of copper. Appl Surf Sci 467:5–11

Zhu B, Xia P, Li Y, Ho W, Yu J (2017) Fabrication and photocatalytic activity enhanced mechanism of direct Z-scheme g-C3N4/Ag_2WO_4 photocatalyst. Appl Surf Sci 391:175–183. https://doi.org/10.1016/j.apsusc.2016.07.104

Zubir NA, Yacou C, Motuzas J, Zhang X, Diniz da Costa JC (2014) Structural and functional investigation of graphene oxide–Fe_3O_4 nanocomposites for the heterogeneous Fenton-like reaction. Sci Rep 4:4594. https://doi.org/10.1038/srep04594